

range of cellular processes, such as divalent ion homeostasis [5–7], cell proliferation [8], neurotransmitter release [9, 10], and cytoskeletal regulation [11, 12]. Global TRPM7 deletion in animal studies revealed that the channel is essential for proper embryonic development [6, 13]; however, its role in neuronal development remains unknown.

The directional outgrowth of neurites is the key process that occurs at every stage of neuronal development [14]. Neurite outgrowth is dependent on dynamic changes of cytoskeleton within the growth cone, which in turn are dependent on local intracellular Ca^{2+} dynamics [15–17]. Intracellular Ca^{2+} transients differing in amplitude, frequency, and entry route have various effects on neurite elongation and motility [18, 19]. F-actin, a major cytoskeletal component, plays an integral role in growth cone motility and navigation [20], and α -actinin-1, a microfilament protein, anchors F-actin to the membrane [21]. Cross-linking of actin filaments by α -actinin-1 purified from HeLa cells is prevented by intracellular free Ca^{2+} [21]. In neurons, a mutation in doublecortin (*Dcx*) gene caused a decrease in α -actinin-1 expression, dysregulation in F-actin distribution, and deficient axon guidance [22]. TRPM7 channels are calcium-permeable and play a role in cell adhesion, cytoskeletal regulation, and intracellular divalent ion homeostasis [2]. These processes are crucial in neuronal development and maturation. Therefore, we asked whether TRPM7 channels are involved in regulation of neuronal development. A recent study identified waixenicin A [23] as a highly potent and specific inhibitor of TRPM7. Waixenicin A blocks the conductance of heterologously expressed TRPM7 channels with an IC_{50} of 16 nM in a magnesium-dependent manner, without affecting other closely related TRPM channels (TRPM2, TRPM4, TRPM6) [23]. The discovery of waixenicin A provides a convenient tool to study the functional role of TRPM7.

Here, we took advantage of the new TRPM7 blocker, waixenicin A, together with gene silencing to investigate the role of TRPM7 in neuronal morphology in mouse hippocampal culture. We demonstrate that TRPM7 regulates axonal growth in a calcium-dependent manner and interacts with F-actin and α -actinin-1. Our study indicates a critical role of TRPM7 in development of hippocampal neurons in culture.

Materials and Methods

Dissociated Cultures

All procedures were performed in accordance with animal welfare guidelines at the University of Toronto and were approved by the institutional animal care and use committee. Embryonic hippocampal cultures were prepared from E16 CD1 mice, as described previously

[4]. Dissected hippocampi were digested with 0.025 % trypsin/EDTA at 37 °C for 15 min. Cell density was determined using an Improved Neubauer hemocytometer, and 1.0×10^4 cells were plated on poly-D-lysine-coated glass coverslips (Sigma) (12 mm no. 1 German Glass, Bellco cat. no. 1943-10012). The cells were kept in 5 % CO_2 at 37 °C in serum-free culture medium (Neurobasal medium supplemented with 1.8 % B-27, 2 % HEPES, 0.25 % Glutamax, and 1 % antibiotic-antimycotic).

Infection of Hippocampal Neurons with Viral TRPM7 shRNA

The viral delivery of small hairpin RNA (shRNA) was used to knock down TRPM7 channels in neurons, as described previously [4]. The small hairpin sequence (shRNA) targeting murine TRPM7 corresponded to the coding regions 5152–5172 relative to the first nucleotide of the start codon of murine TRPM7 (GeneBank accession number AY032951). The sequence was packaged in a recombinant serotype 1 adeno-associated virus (rAAV_{TRPM7}) with enhanced green fluorescent protein (EGFP) [4]. Two controls were either packaged with a mismatch negative control siRNA sequence (rAAV_{shSCR}) or with EGFP alone (empty vector, rAAV_{EGFP}). Cultures were treated at day in vitro 1, 4 h after plating the cells, with 3.23×10^{12} , 3.70×10^{12} , and 3.64×10^{12} genomes of rAAV_{shTRPM7}, rAAV_{shSCR}, or rAAV_{EGFP} respectively.

Drug Treatment of Hippocampal Neurons

Waixenicin A was obtained from freeze-dried polyps of the soft coral *Sarcothelia edmondsoni*, which was collected in Kailua Bay (Oahu, Hawaii). The biological material was ground and exhaustively extracted with hexane. The solvent was removed under vacuum to give a crude extract residue. The residue was first fractionated by silica high-performance liquid chromatography (HPLC) to give semi-purified waixenicin A. Final purification was accomplished by reversed phase (C_{18}) HPLC, and compound identity and purity was established by nuclear magnetic resonance spectroscopy (NMR, d_6 -benzene) in comparison to in-house reference data [23]. Aliquots of the compound were stored as a dried film in that were stored in a dessicator until use. The stock of waixenicin A was prepared by dissolving the compound in 100 % methanol and adding phosphate-buffered saline (PBS) to dilute methanol to 2.5 % concentration. Waixenicin A was added to cell cultures on day in vitro (DIV) 2, 24 h post-plating. Control neurons were either untreated or treated with methanol at the highest concentration used in the waixenicin A treatment.

Calcium Imaging

Intracellular calcium ($[Ca^{2+}]_i$) was measured using a Fura-2 ratiometric Ca^{2+} imaging system as described previously [24]. Neurons were pre-loaded with Fura-2 AM (2 μ M) in dark for 30 min at room temperature. Fura-2 calcium signal was acquired at alternate excitation wavelengths of 340 and 380 nm by a Deltaram V single monochromator controlled by EasyRatioPro (PTI), while neurons were perfused with control solution containing (mM) 129 NaCl, 2 $CaCl_2$, 1 $MgCl_2$, 25 HEPES, 30 glucose, and 5 KCl (with pH of 7.3–7.4 and osmolality ranging from 320 to 330 mOsm), or low Mg^{2+}/Ca^{2+} solution (0 $MgCl_2$, 0.5 $CaCl_2$) with or without 500 nM waixenicin A. Signals were digitized by an intensified charged-coupled device (ICCD) camera (PTI), and fluorescence intensity (Poenie-Tsien) ratios of images were calculated by using EasyRatioPro.

Electrophysiology

Whole-cell TRPM7-like currents were recorded from DIV3 to DIV7 cultured mouse hippocampal neurons as described previously [4], using symmetrical reverse voltage ramps from +100 to –100 mV (100 ms) with the holding potential of –100 mV. The pipette solution contained 140 mM CsF, 35 mM CsOH, 10 mM HEPES, 2 mM tetraethylammonium chloride (TEA-Cl), 11 mM EGTCA, 1 mM $CaCl_2$, 2 mM $MgCl_2$, and 2 mM K_2ATP (pH 7.3, 290–300 mOsm/L) [25]. The extracellular solution contained 140 mM NaCl, 5 mM KCl, 2 mM $CaCl_2$, 20 mM HEPES, 500 nM tetrodotoxin (TTX), 25 μ M D-(–)-2-amino-5-phosphonopentanoate (APV, Abcam), 40 μ M 6-cyano-7-nitroquinoxaline-2,3-dione (CNQX, Tocris), 5 μ M nimodipine (Sigma), and 10 mM glucose, pH adjusted to 7.4 (NaOH) [4].

Immunocytochemistry

Neurons were fixed with pre-warmed 4 % paraformaldehyde/4 % sucrose in PBS for 15 min, permeabilized with 0.1 % Triton X-100 in PBS for 10 min, and blocked with a blocker solution (2 % bovine serum albumin, 2 % fetal bovine serum, and 0.2 % fish gelatin in PBS) for 1 h at room temperature, as described previously [4]. Cells were then incubated the primary antibodies, including a mouse monoclonal anti- α -tubulin antibody (1:1000, Sigma, no. T-5168), a goat polyclonal anti-TRPM7 (1:200, Abcam, Ab729), a mouse monoclonal anti- α actinin (1:500, Abcam, Ab18061), or a mouse monoclonal anti-NeuN (1:500, Millipore, no. MAB377). To differentiate between axons and dendrites, neurons were incubated with mouse monoclonal anti-tau-1 (axonal marker; 1:500, Millipore, MAB3420) and chicken polyclonal anti-microtubule associated protein 2 (MAP2) (dendritic marker; 1:500, Millipore, Ab15452).

Image Acquisition for Neurite Length Analysis

Images of neurons were captured with either a Leica TCS LS confocal laser-scanning microscope (Heidelberg, Germany; Leica confocal software, version 2.5; build 1347; Leica Microsystems) with either $\times 40$ (NA 1.25) or $\times 63$ (NA 1.32) oil immersion lenses, and 488-, 543-, and 633-nm lasers, as described previously [26], or a Carl Zeiss confocal laser scanning microscope LSM700 with either $\times 63$ DIC (NA 1.40) or $\times 40$ DIC (NA 1.3) oil immersion lenses, and 405-, 488-, and 543-nm lasers [4]. Each Z-plane was 0.3 μ m. All cells were imaged using the same magnification and laser settings. All cells were imaged at a resolution of 1024×1024 pixels using the same magnification and laser settings.

Neurite Length Analysis

Analysis of neurite length of shRNA-treated neurons was carried out by semi-manually tracing the neurites of neurons in the maximally projected confocal images ($\times 40$ lens) using the NeuronJ plugin (www.imagescience.org/meijering/software/neuronj) for ImageJ. Each traced neurite was labeled by the order of branching (by primary, secondary, and tertiary or greater) to get the number of neurites. Neurons treated with waixenicin A were analyzed with SynD, a semi-automated image analysis routine [27]. For neurons (DIV >6) that require a larger field of view to capture a single neuron, multiple images were taken under the $\times 40$ lens first and mosaics of overlapping images were assembled in ImageJ (NIH, <http://rsb.info.nih.gov/ij>) using MosaicJ plugin before neurite length analysis.

Protein Colocalization Analysis

Confocal images of cells that were triple-stained with antibodies targeting the proteins of interest were scanned at a resolution of 2048×2048 pixels using a $\times 63$ (NA 1.40) oil immersion lens (Zeiss LSM700). Each fluorescence signal was imaged separately with corresponding channel, without pixel saturation. Protein colocalization was estimated by quantifying the degree of overlap between the fluorescence intensities in the each pixel located in the region of interest (ROI). For each image, an ROI was selected in the cell body, neurite, growth cone, and a background area (outside of the cell) to be used as the control. A Pearson's correlation coefficient (Rr) was measured using an ImageJ plugin called the intensity correlation analysis, as described previously [26]. The Rr value of 1.0 indicates close colocalization, and 0 indicates low probability for colocalization.

Coimmunoprecipitation

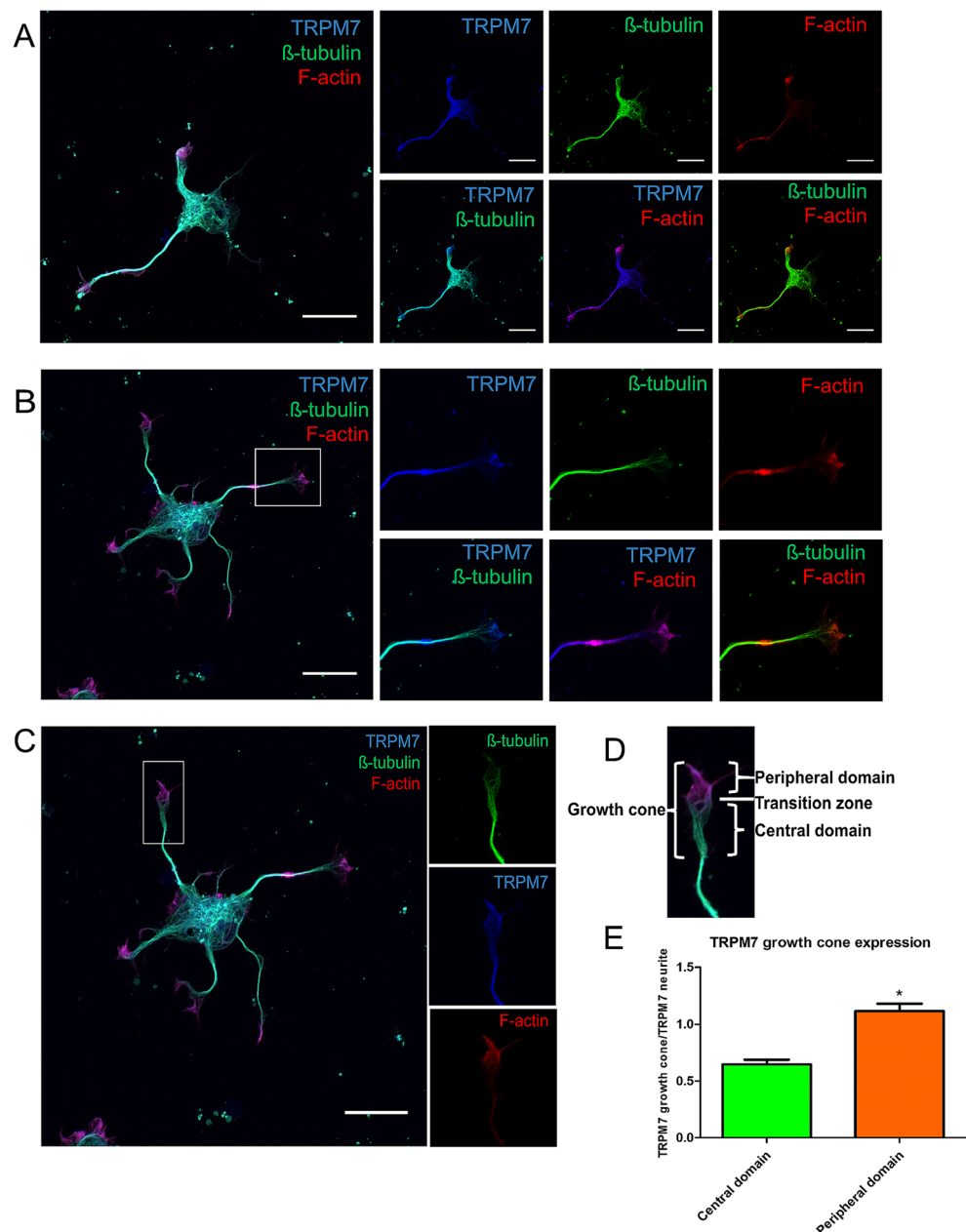
Protein isolated from MDA-MB-231 cells (250 μ g) (Sigma-Aldrich) in RIPA lysis buffer (Santa Cruz Biotechnology, sc-24948) was incubated with 2 μ g of anti-TRPM7 antibody (Abcam, ab85016) for 90 min at 4 °C and 10 min at room temperature (RT). Then, 20 μ l of pre-washed Protein A/G PLUS-Agarose beads (Santa Cruz Biotechnology, sc-2003) were added, and the mixture was incubated and shaking at 4 °C overnight. The protein mixture was vortexed, heated from 5 min, and centrifuged for 10 min at 3000 rpm. The supernatant

was collected and run sodium dodecyl sulfate polyacrylamide gel electrophoresis (SDS-PAGE).

Protein Identification by Mass Spectrometry

LC-MS/MS and protein identification were performed as described previously [28]. In-gel trypsin digestion of proteins was performed using an In-gel Tryptic Digestion Kit (Pierce, Thermo Fisher Scientific Inc., Rockford, IL, USA). Peptides were sent to the Ontario Cancer Biomarker Network Facility Centre for protein identification by nano LC/MS/MS HPLC chromatographic separation. Mascot Generic and Mascot

Fig. 1 TRPM7 expression pattern in DIV2 hippocampal neurons. **a** DIV2 hippocampal neuron triple-stained with antibodies recognizing α -tubulin (green) and TRPM7 (blue) and rhodamine phalloidin for F-actin (red). two-image and three-image overlays were included to show the relative distribution of TRPM7 with respect to cytoskeletal structures. **b, c** Distribution of TRPM7 and cytoskeletal proteins in two separate growth cones. **d** Schematic of the domains within the growth cone. **e** Ratio of TRPM7 intensities in central and peripheral domains of the growth cone to TRPM7 intensity in the neurite; $n=5$ neurons, $n=9$ growth cones. Scale bars are 20 μ m



Daemon were used to combine and analyze data. After the MS/MS Ions Search against UniProt Universal Protein Resources knowledge base (<http://www.uniprot.org/>), a protein was accepted as identified if the total Mascot score was greater than the significance threshold.

Western Blotting

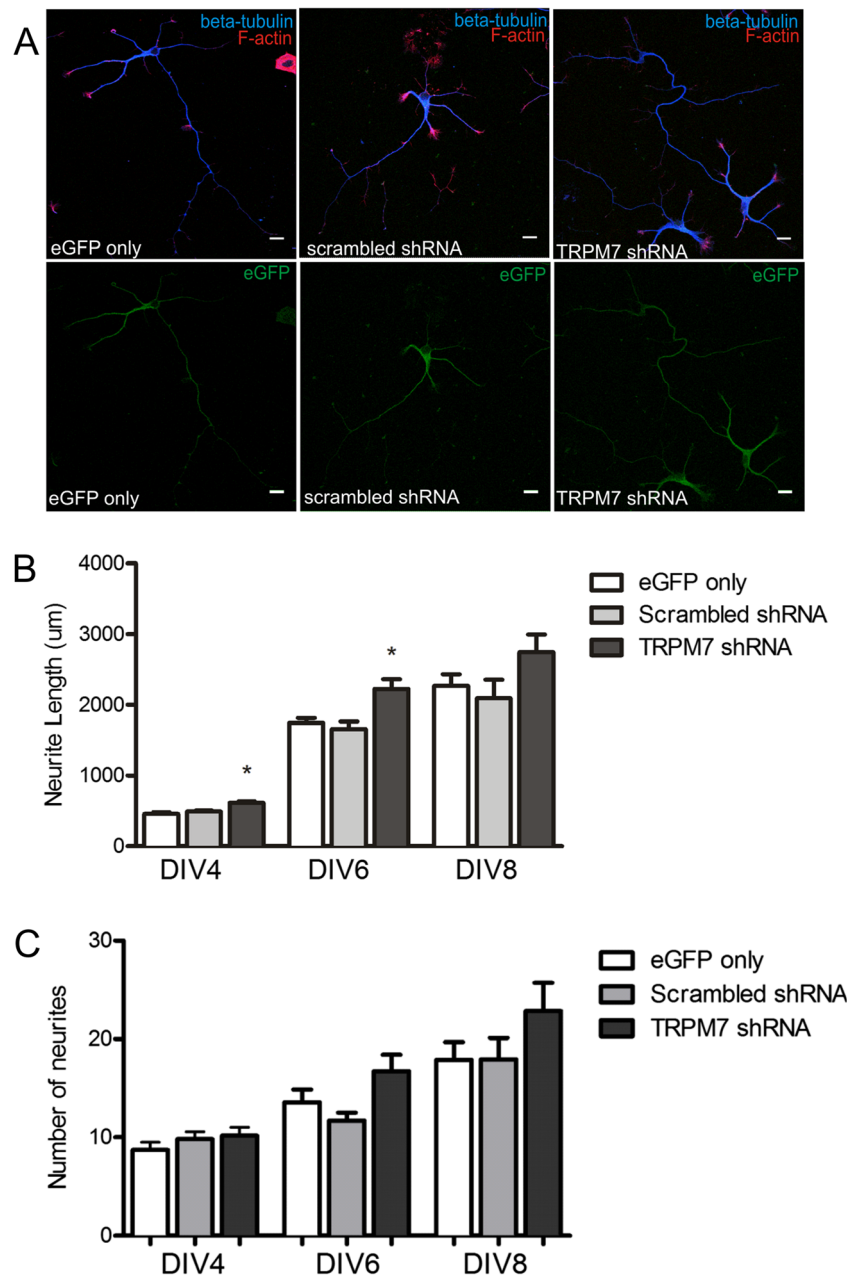
The protein was collected from dissociated mouse hippocampal neuronal cells or MDA-MB-213 cells in RIPA buffer (Santa Cruz Biotechnology, sc-24948) with protease inhibitor mixture (Santa Cruz Biotechnology, sc-29131). The protein samples (15 $\mu\text{g}/\text{well}$) were run on 8 % Tris-glycine gel.

Membranes were incubated with specific primary antibodies against α -actinin (1:1000; Abcam, ab18061) and GAPDH (1:1000; Cell Signaling, 14C10) at 4 °C overnight. Antibody-labeled protein bands were visualized using chemiluminescent reagents (PerkinElmer) and analyzed by exposure to film (HyBlot CL).

Statistical Analysis

Data are presented as the mean \pm SEM. Statistical analysis was performed using GraphPad Prism (GraphPad Software, San Diego, CA). The multiple comparisons of means between experimental and control conditions were performed with

Fig. 2 TRPM7 knockdown with shRNA increases total neurite outgrowth and length of the longest neurite. **a** Representative confocal image overlays (*top panel*) and eGFP signal (*bottom panel*) of DIV4 hippocampal neurons infected with different AAV-1 constructs. **b** Total neurite length and **c** total number of neurites per neuron. For groups at DIV4: eGFP only $n=42$, scrambled shRNA $n=43$, TRPM7 shRNA $n=48$; for groups at DIV6: eGFP only $n=26$, scrambled shRNA $n=40$, TRPM7 shRNA $n=35$; for groups at DIV8: eGFP only $n=25$, scrambled shRNA $n=20$, TRPM7 shRNA $n=23$. Data are shown as mean \pm SEM. Statistical analysis: one-way ANOVA with Bonferroni post hoc; $*p<0.05$. Scale bars are 20 μm



Bonferroni post hoc test following the one-way ANOVA. Values of $p < 0.05$ are taken as statistically significant.

Results

TRPM7 Protein Is Expressed in Neurites and Growth Cones of Cultured Hippocampal Neurons

Earlier studies have shown that TRPM7 protein is extensively expressed in hippocampal neurons in both rat brain slices [4] and rat or mouse primary cell cultures [25]. Here, we first investigated the distribution of TRPM7 in the growth cone region of the cultured hippocampal neurons dissociated from E16 embryonic CD1 mice. Confocal immunofluorescence imaging revealed that TRPM7 channels are present in growth cones of DIV2 hippocampal neurons (Fig. 1b), in addition to the somata and processes (Fig. 1a).

To further characterize the distribution of TRPM7 relative to cytoskeletal structures, hippocampal neurons were triple-labeled with anti-TRPM7, anti- β -tubulin, and rhodamine phalloidin for filamentous actin (F-actin). High magnification confocal images showed the relation between the spatial distribution of TRPM7 to two cytoskeletal structures, β -tubulin, and F-actin (Fig. 1a). In the central microtubule-containing domain of the growth cone, TRPM7 expression was low, as evident by the lower fluorescent intensity. In the peripheral domain containing filopodia and lamellipodia, TRPM7 channels are highly expressed along the actin bundles (Fig. 1b, c). Further quantification of TRPM7 fluorescence intensity showed higher expression of TRPM7 in the periphery of the growth cone, where filopodia are located (Fig. 1c–e). As actin dynamics determines growth cone motility and is necessary for directed axonal outgrowth [29], our results suggest that TRPM7 may mediate axonal outgrowth through actin regulation.

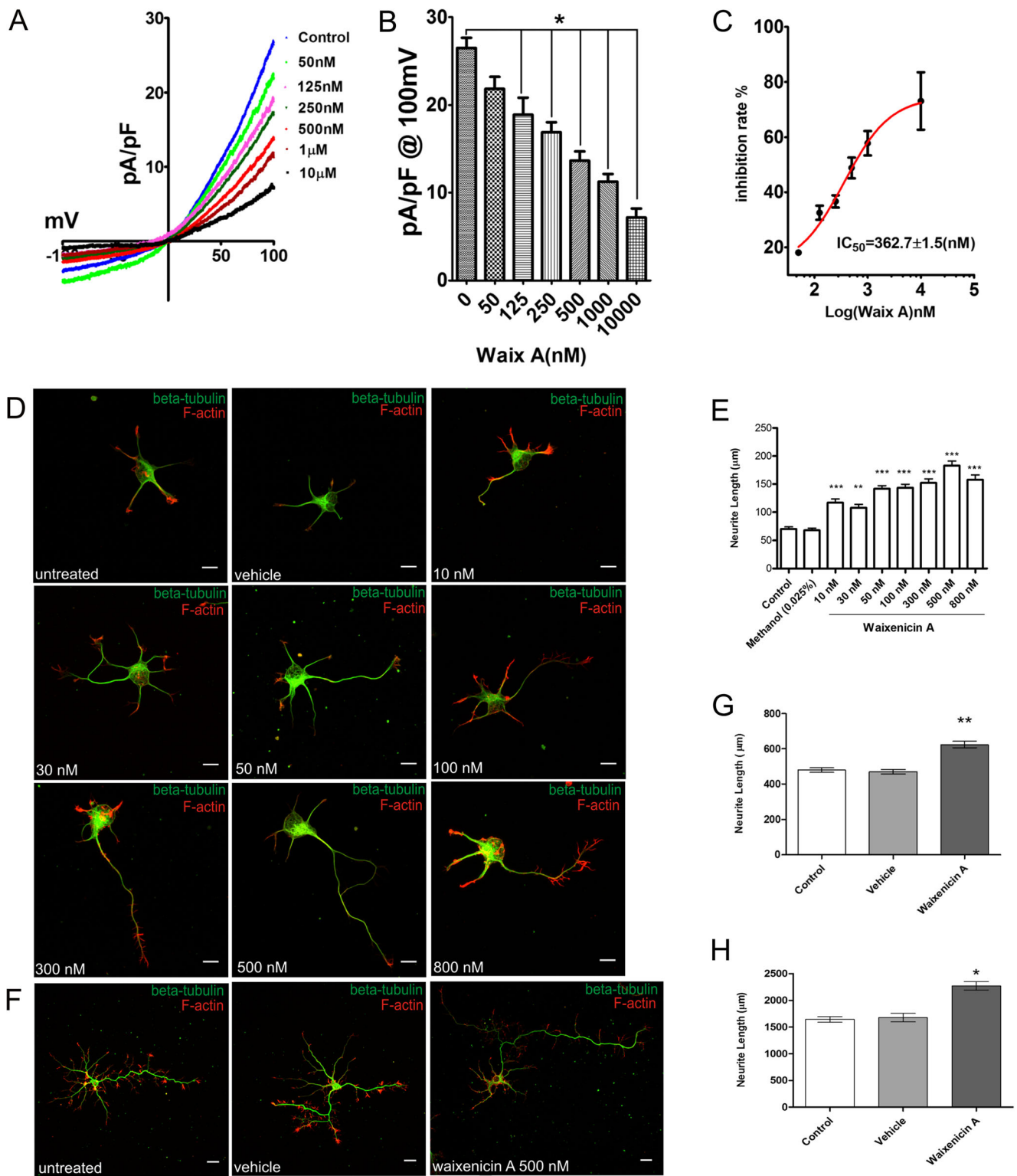
TRPM7 Suppression Enhances Neurite Outgrowth of Cultured Hippocampal Neurons

To test the involvement of TRPM7 in neuronal outgrowth, we first used an RNA interference approach to study whether reduction of the TRPM7 level affects the outgrowth pattern of hippocampal neurons. AAV-1-based vectors, eGFP-control, eGFP-shRNA control, and eGFP-TRPM7-shRNA were each applied to hippocampal culture, as reported in previous study [4]. The efficiency of TRPM7 knockdown was confirmed by measuring relative fluorescent level of TRPM7 against NeuN (neuronal specific nuclear protein) in GFP-expressing neurons, and TRPM7 was reduced by 65 % compared to neurons expressing eGFP only or control shRNA (Supplementary Fig. 1c, d), consistent with the previous study [4].

Fig. 3 Waixenicin A inhibits TRPM7 activity in a dose-dependent manner and enhances total neurite outgrowth of hippocampal neurons and different time points in culture. **a** Mean currents of TRPM7 in DIV3–DIV7 hippocampal neurons without or with different concentration waixenicin A (*Waix A*) (50 nM, $n=6$; 125 nM, $n=7$; 250 nM, $n=13$; 500 nM, $n=11$; 1000 nM, $n=8$; 10,000 nM, $n=3$) incubation. **b** Mean outward current measured at 100 mV on control (0 nM *Waix A*, $n=27$) and different concentrations of *Waix A* treatments (30-min incubation time on hippocampal neurons) (50 nM, $n=6$; 125 nM, $n=7$; 250 nM, $n=13$; 500 nM, $n=11$; 1000 nM, $n=8$; 10,000 nM, $n=3$), respectively ($*p < 0.05$ vs control, one-way ANOVA). **c** Non-linear curve fitting analysis for the inhibition rate of *Waix A* on TRPM7 currents at 100 mV. It indicated that the IC_{50} of *Waix A* for TRPM7 current in hippocampal neurons is 362.7 ± 1.5 nM. **d** Representative images of DIV2 control, vehicle control neurons, and neurons treated with increasing doses of *Waix A* stained for β -tubulin (*green*) and F-actin (*red*). *Scale bars* are 10 μ m. **e** Total neurite length of DIV2 neurons (control $n=81$; vehicle $n=78$; waixenicin A 10 nM $n=62$, 30 nM $n=76$, 50 nM $n=84$, 100 nM $n=98$, 300 nM $n=84$, 500 nM $n=96$, 800 nM $n=74$). **f** Representative images of hippocampal neurons DIV6. **g** Total neurite length of DIV3 neurons (control $n=104$, vehicle $n=99$, waixenicin A $n=96$). **h** Total neurite length of DIV6 neurons (control $n=87$, vehicle $n=71$, waixenicin A $n=76$). For DIV3 and DIV6 neurons, waixenicin A dose was 500 nM. Data are shown as mean \pm SEM. Statistical analysis: one-way ANOVA with Bonferroni post hoc; $*p < 0.05$, $**p < 0.01$, $***p < 0.001$. All *scale bars* are 20 μ m

To capture the effects of suppressing TRPM7 on neurons as early as possible, the neurons were infected 4 h after plating. The cells expressing eGFP, a sign of successful infection, were monitored on DIV4, DIV6, and DIV8. As can be seen from representative images of neurons on day DIV4, neurons with TRPM7 knockdown (shTRPM7) had similar morphological patterns of neurite development compared to the control neurons (Fig. 2a). However, they consistently showed a greater total neurite length per neuron at all time points (DIV4, 615.5 ± 30.3 μ m, $n=48$; DIV6, 2416.0 ± 179.8 μ m, $n=35$; and DIV8, 2842.0 ± 238.3 μ m, $n=23$) than the neurons treated with the control shSCR (DIV4, 490.1 ± 25.3 μ m, $n=43$; DIV6, 1633.0 ± 82.1 μ m, $n=40$; and DIV8, 2117 ± 205.2 μ m, $n=20$) or eGFP (DIV4, 458.9 ± 32.4 μ m, $n=42$; DIV6, 1744 ± 69.8 μ m, $n=26$; and DIV8, 2267 ± 163.5 μ m, $n=19$) (Fig. 2b). The branching and total number of neurites did not differ significantly between the groups at all three time points (Fig. 2c). Moreover, further in-depth analysis revealed that the number of primary, secondary, and tertiary dendrites (Supplementary Fig. 2a) did not differ significantly between groups and all three time points either (Supplementary Fig. 2b–d).

Here, we demonstrate that TRPM7 channels may negatively regulate neuronal outgrowth. RNA interference reduced expression level of the TRPM7 channels in a cell, so it is not clear whether the enhanced axonal elongation in TRPM7 knockdown is due to a physical decrease in the channel protein level or channel activity. In light of the discovery of the new TRPM7 channel blocker, we next used pharmacological approach to study the involvement of TRPM7 activity in neuronal outgrowth.



Waixenicin A, A Novel Blocker of TRPM7 Channels, Preferentially Enhances Axonal Growth of Cultured Hippocampal Neurons

Waixenicin A is a newly identified specific TRPM7 inhibitor and blocks the activity of either recombinant channel

or native channel in RBL-1 cells [23]. We investigated whether waixenicin A blocks ion conductance of TRPM7 and affects axonal outgrowth in hippocampal culture. Our whole-cell patch-clamp recording showed that waixenicin A decreased the TRPM7-like current in DIV3–DIV7 hippocampal neurons in a dose-dependent manner (Fig. 3a, b),

with an IC_{50} value of 362.7 ± 1.5 nM (Fig. 3c). The TRPM7-like current was recorded with a ramp protocol in the presence of tetrodotoxin (TTX), D-(-)-2-amino-5-phosphonopentanoate (APV), CNQX, and nimodipine in the bath solution to block the activation of voltage-gated Na^+ , NMDA, non-NMDA glutamate-activated, and L-type Ca^{2+} voltage-gated channels, respectively [4].

We next examined whether pharmacological inhibition of TRPM7 activity is sufficient to affect neurite outgrowth, similar to TRPM7 viral knockdown. This approach also allowed us to examine the morphological changes in the early stages in culture, something that was not feasible in shRNA study. Various concentrations of waixenicin A (10, 30, 50, 100, 300, 500, and 800 nM) and 0.025 % of methanol (vehicle control) were added to hippocampal culture on DIV2, 24 h after plating. Neurons were stained for two major cytoskeletal components, β -tubulin and F-actin, 6 h post-treatment to visualize the morphology of the cells (Fig. 3d). Compared to control neurons, neurons treated with waixenicin A exhibited significant increases in total neurite length with 500 nM being the most effective dose (Fig. 3e). Moreover, neurons treated with 500 nM of waixenicin A 24 h after plating exhibited substantial increases in outgrowth as compared to the untreated control or vehicle control neurons 24 and 96 h post-treatment, on DIV3 and DIV6. Representative images of DIV6 neurons are presented in Fig. 3f. The total neurite lengths per neuron enhanced significantly in waixenicin A group on both DIV3 (control, 479.2 ± 13.6 μ m, $n=104$; vehicle, 470.1 ± 16.4 μ m, $n=99$; waixenicin A, 624.8 ± 18.6 μ m, $n=96$; $p < 0.01$; Fig. 3g) and DIV6 (control, 1641.8 ± 53.8 μ m, $n=87$; vehicle, 1676.2 ± 94.6 μ m, $n=71$; waixenicin A, 2272.5 ± 78.9 μ m, $n=86$; $p < 0.01$; Fig. 3h). As the increase in total neurite outgrowth could be contributed by increases in axonal length, dendritic length, or both, we next evaluated the effects of TRPM7 channel blockade on axons and dendrites. Neurons were stained for axonal (tau-1) and dendritic (MAP2) markers, and representative images of neurons on DIV4, DIV6, and DIV8 are shown in Fig. 4a–c, respectively. At DIV4, neurons treated with the TRPM7 blocker showed a 71 % increase in axonal length and 33 % increase in dendritic length compared to controls. At DIV6, axonal and dendritic lengths increased by 48 and 25 %, respectively, while at DIV8 axonal length increased by 53 %, and dendritic length increased only by 14 % (Fig. 4d shows axonal lengths, and Fig. 4e shows dendritic lengths). Sholl analysis revealed a consistent increase in branching of axons at all times points while dendrites only showed greater branching on DIV4 and DIV6, but not DIV8. Sholl analysis of axons on DIV4 is shown in

Fig. 4f and dendrites in Fig. 4g. Therefore, we concluded that under normal conditions, TRPM7 is a potential negative regulator of axonal growth.

Blocking TRPM7 Conductance Accelerates the Progression of Cultured Hippocampal Neurons Through Developmental Stages

Dotti et al. [14] described that hippocampal neurons go through five stages of development in culture. Here, we show that our E16 hippocampal cultures closely follow these developmental stages (Fig. 5a). At stage 1, neurons protrude veil-like lamellipodia that explore extracellular environment within ~6 h in culture. The second stage is characterized by appearance of several neurites of similar length (~24 h in culture). Around 36–48 h in culture, neurons move into the third stage, also known as neuronal polarization. At this stage, one of the neurites begins elongating faster than the rest. Molecular marker expression of that neuron also changes, as axon starts to preferentially express tau-1 and dendrites to express MAP2 (Fig. 5b). Stage 4 is characterized by increased branching and development of axons and dendrites (>4 days in culture), and neurons at stage 5 (>14 days in culture) show further maturation of axonal and dendritic arbors and formation of synapses. We outlined the neuronal transition through these stages in Fig. 5a. We focused on the transition between stage 2 and stage 3, as it is crucial for breaking neuronal symmetry and progression toward functionality.

We asked whether TRPM7 channel activity is required for neuronal development. Since the developmental transitional stages take place within the first 3 days in culture, we examined the effects of waixenicin A on the developmental stages from the neurons in DIV2 and DIV3 cultures. As shown in Fig. 5c, blocking TRPM7 activity by waixenicin A shifted the developmental transitional stage toward an early time in culture. At DIV2, untreated and vehicle-treated neuron cultures had 14 and 15 % of neurons in stage 3 (axon distinguished by ICC with anti-tau-1 antibody; dendrites with anti-MAP2 antibody), while neurons treated with 500 nM waixenicin A had 30 % of neurons in stage 3 (Fig. 5c, left). In DIV3 cultures, untreated and vehicle-treated groups showed that 32 and 31 % of neurons progressed into stage 3, while neurons treated with waixenicin A had 54 % neurons in stage 3 (Fig. 5c, right). We have also addressed the progression of neurons from stage 2 into stage 3 quantitatively in a different population of neurons. As stage 3, or neuronal polarization, starts when one of the neurites begins to elongate faster than others, we calculated the difference between the length of the longest neurite and the average length of the remaining neurites (Supplementary Fig. 3a). We found an overall increase in length difference in both DIV2 and DIV3 hippocampal neurons treated with waixenicin A, when compared to control groups, suggesting an increase in the rate of axonal growth, an increase in the

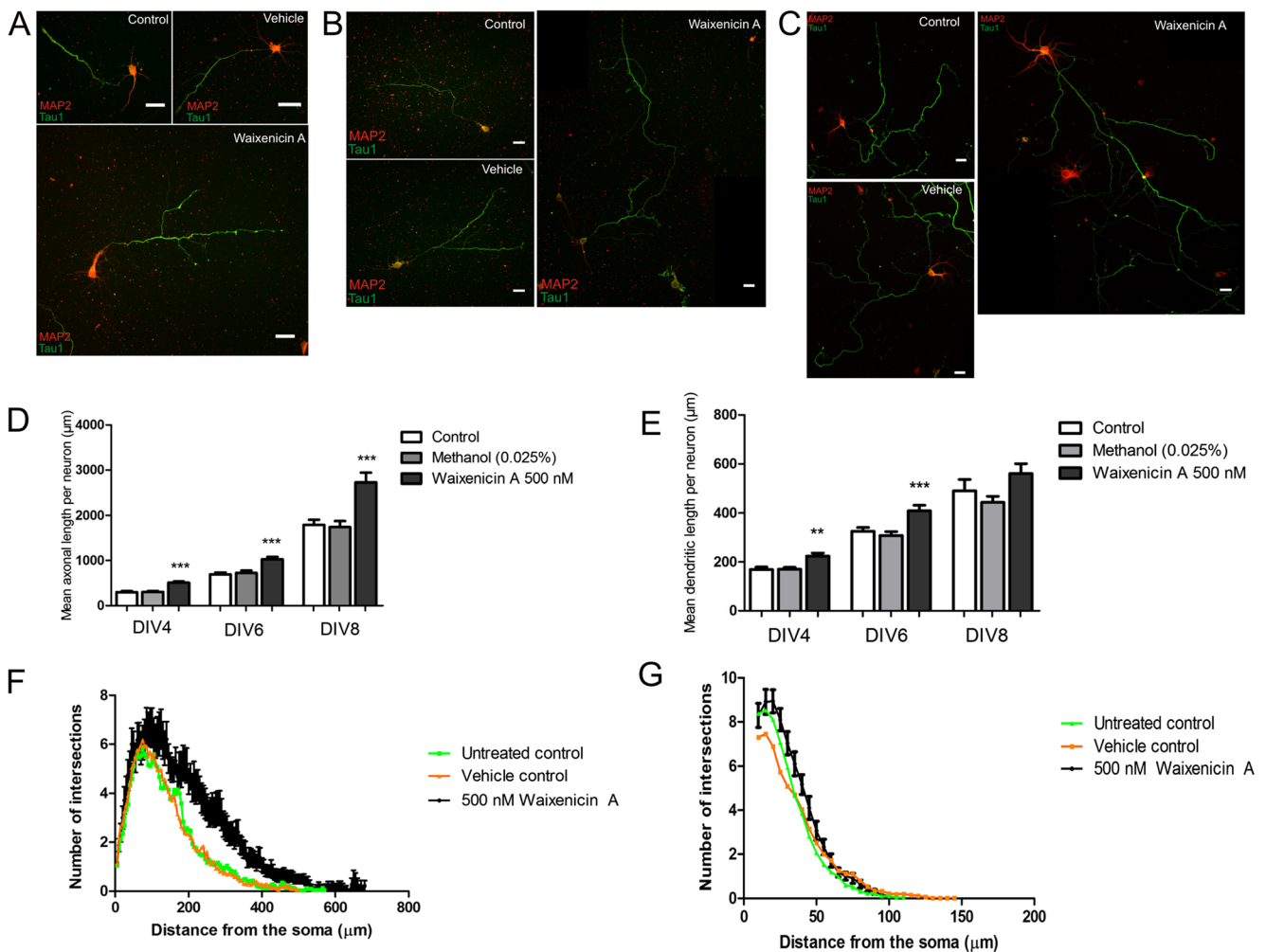


Fig. 4 Waixenicin A treatment enhances outgrowth and branching of axons and dendrites. **a–c** Representative images of neurons in different treatment groups on DIV4, DIV6, and DIV8. **d** Average axonal and **e** dendritic lengths of DIV4 (control $n=56$, vehicle $n=83$, waixenicin A $n=59$), DIV6 (control $n=50$, vehicle $n=46$, waixenicin A $n=49$), and DIV8 (control $n=50$, vehicle $n=49$, waixenicin A $n=32$) neurons. **f** Sholl

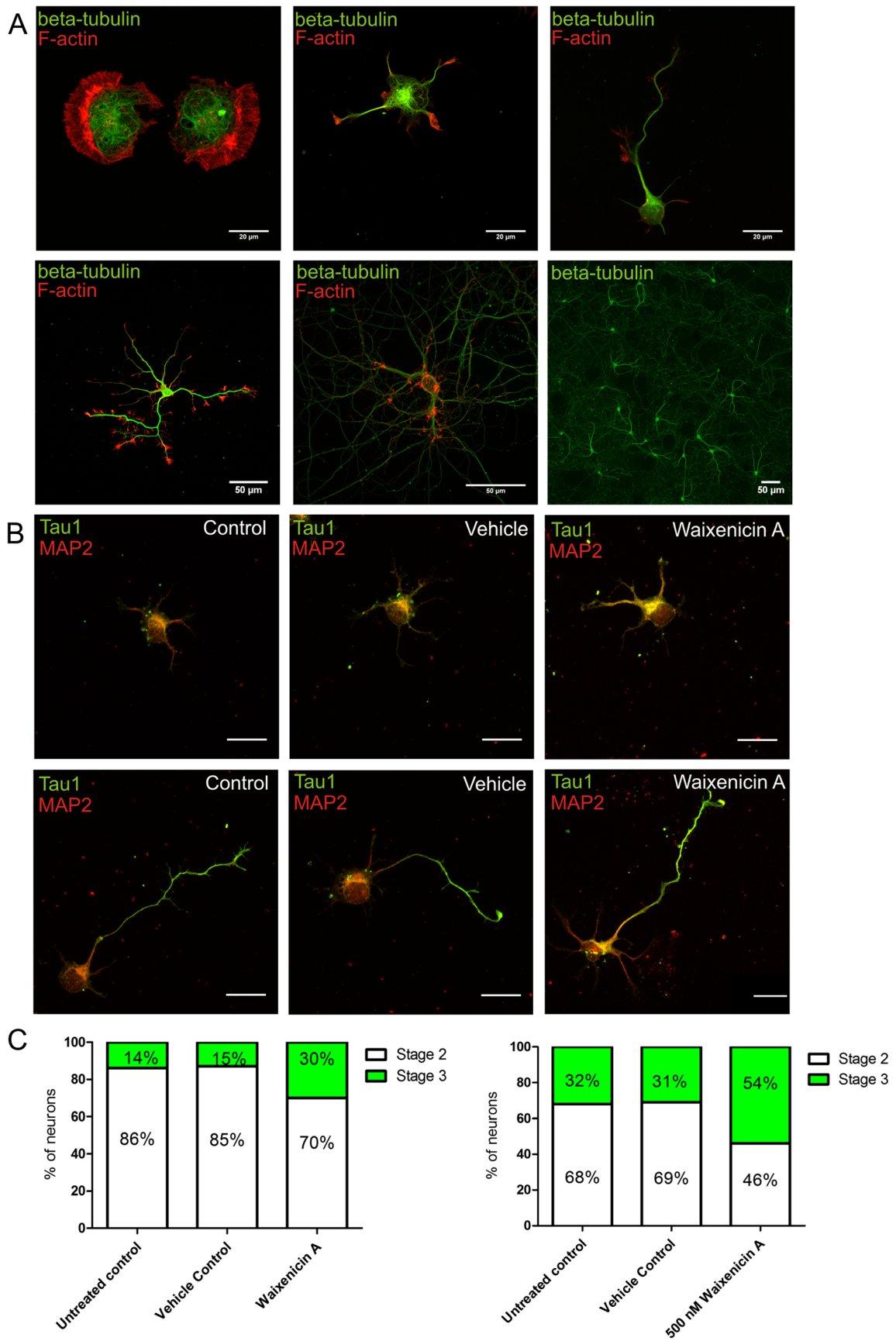
analysis of axons of DIV8 neurons indicates increased branching and length of branches with waixenicin A treatment (control $n=50$, vehicle $n=49$, waixenicin A $n=32$). **g** Sholl analysis of dendrites of DIV8 neurons showed increased number of branches only ($n=31$). Data are shown as mean \pm SEM. Statistical analysis: one-way ANOVA with Bonferroni post hoc; ** $p<0.01$, *** $p<0.001$

number of stage 3 neurons or both (Supplementary Fig. 3b). Upon further investigation, we found that the length difference of neurons that were morphologically defined as stage 2 was significantly lower than that of neurons morphologically defined as stage 3, yet remained consistent between different groups (DIV2 stage 2: untreated control 0.44 ± 0.02 , vehicle control 0.5 ± 0.02 , waixenicin A 0.05 ± 0.02 ; DIV3 stage 2: untreated control 0.52 ± 0.02 , vehicle control 0.54 ± 0.02 , waixenicin A 0.58 ± 0.02 ; DIV2 stage 3: untreated control 0.77 ± 0.02 , vehicle control 0.74 ± 0.03 , waixenicin A 0.84 ± 0.02 ; DIV3 stage 3: untreated control 0.81 ± 0.02 , vehicle control 0.86 ± 0.02 , waixenicin A 0.87 ± 0.02), suggesting that there are more stage 3 neurons in waixenicin A-treated group, while the rate of axonal elongation does not change between the groups. Based on these data, we defined a neuron to be in stage 3 if the difference between the length of its longest

neurite and the average length of the remaining neurites is greater or equal to 0.67. Based on this definition, we have found that untreated control, vehicle control, and waixenicin A-treated neurons had 15, 15, and 33 % of neurons in stage 3 at DIV2 and 35, 32, and 53 % at DIV3, respectively, and that these data correspond well with our morphological data. These findings suggest that TRPM7 plays a role in inhibiting premature transition between the developmental stages under normal conditions and thus regulates neuronal maturation.

TRPM7 Knockdown and Waixenicin A Decrease Calcium Influx Detected by Fura-2 Calcium Sensitive Dye

Lowering extracellular concentrations of divalent cations, such as Mg^{2+} , potentiates calcium influx through TRPM7 channels [4]. To test if TRPM7 knockdown reduces the influx



◀ **Fig. 5** Treatment with waixenicin A promotes maturation of hippocampal neurons. **a** Representative images of developmental stages of hippocampal neurons according to Dotti et al. *Top panel*: stage 1 (*left*), stage 2 (*center*), and stage 3 (*right*). *Bottom panel*: stage 4 (*left*) and stage 5 (*center and right*). **b** Representative images of neurons in stage 2 (*top panel*) and stage 3 (*bottom panel*) in different treatment groups. Scale bars are 20 μm . **c** Proportion of neurons in stages 2 and 3 in different treatment groups. *Left panel*: DIV2 cultures (6 h post-treatment; $n=137$); *right panel*: DIV3 cultures (24 h post-treatment; $n=144$). Chi-squared: DIV2 untreated control versus waixenicin A, $p=0.006$; DIV3 untreated control versus waixenicin A, $p=0.04$

of calcium in hippocampal neurons, we carried out ratiometric Fura-2 Ca^{2+} imaging at various extracellular Mg^{2+} concentrations. In control neurons (scrambled shRNA), the Mg^{2+} -free and low Ca^{2+} condition induced a net increase of the Fura-2 Ca^{2+} signal (ratio for exCitation at 340/380 nm) by 0.08 ± 0.003 ($n=16$) (Fig. 6b, left panel). In neurons treated with TRPM7 shRNA, the low Mg^{2+} -induced Ca^{2+} signal was significantly reduced to 0.03 ± 0.004 ($n=16$, $p<0.05$) (Fig. 6b, middle panel), a $62 \pm 4\%$ ($n=16$) decrease from control value (Fig. 6b, right panel). Representative images of neurons treated with scrambled shRNA and TRPM7 shRNA are shown in Fig. 6a. KCl (40 mM) was applied at the end of every recording to confirm that the neurons are still responsive. No significant difference was seen in the amplitude of KCl-induced Ca^{2+} spike between the groups. These results suggest that knockdown of TRPM7 reduces the low divalent cation-induced Ca^{2+} influx through TRPM7 channels in hippocampal neurons.

We next examined whether the observed Ca^{2+} influx could be blocked by waixenicin A. Fura-2 Ca^{2+} signals were monitored under the same Mg^{2+} -free and low Ca^{2+} condition in the absence or presence of 500 nM waixenicin A. In the presence of waixenicin A, the net increase of the Ca^{2+} signal was 0.03 ± 0.004 ($n=10$, $p<0.05$), which was significantly lower than that recorded in the absence of waixenicin A (0.09 ± 0.008 , $n=10$, $p<0.05$) (Fig. 6d, left panel). The decrease was $58 \pm 8\%$ ($n=10$) from control value (Fig. 6d, right panel). The KCl-evoked Ca^{2+} signal was not significantly different between the two groups. Representative images are shown in Fig. 6c. Two consecutive applications of Mg^{2+} -free and low Ca^{2+} solution did not produce a desensitization of the calcium signal (Fig. 6e). Taken together, waixenicin A suppressed the free Mg^{2+} -induced Ca^{2+} influx through TRPM7 channels in hippocampal neurons, consistent to that seen with TRPM7 knockdown.

TRPM7 Channels Interact with α -Actinin-1 and F-Actin

To explore the mechanisms underlying the effect of TRPM7 on neuronal growth, we carried out affinity pull-down assay using TRPM7 channel protein antibody in hippocampal proteins, followed by 1D SDS-PAGE and mass spectrometry to

search for potential binding partners of TRPM7 channel protein. The potential binding partners were identified by ESI-TRAP MS in combination with database analysis, as described previously [28]. We found both α -actinin-1 and F-actin in the TRPM7-binding protein complex (Fig. 7a). TRPM7-to-actin or TRPM7-to-actinin binding was further confirmed by coimmunoprecipitation (co-IP) assays with proteins isolated from MDA-MB-231 cells, a breast cancer cell line with high TRPM7 expression [30]. As shown in Fig. 7b, both α -actinin-1 and F-actin were found in the TRPM7 binding protein complex.

We then conducted the quantitative colocalization analysis to determine the degree of overlap between TRPM7 and α -actinin-1 or F-actin at the same pixel location on the multi-channel fluorescence images. Colocalization of fluorescent signals suggests a high probability of two antigens cooccurring in close proximity, indicated by Pearson's correlation coefficient (Rr; one signifies a high degree of colocalization, and zero indicates low likelihood of localization) [26]. The colocalization of TRPM7 and α -actinin-1 or F-actin was focused within the lamellipodia (mesh-like structures) and filopodia (filamentous structures) of the neuronal growth cones. The Rr for TRPM7 and α -actinin was 0.59 ± 0.02 in filopodia ($n=22$) and 0.43 ± 0.04 in lamellipodia ($n=22$) in the normal culture condition. Rr values for TRPM7 and F-actin were 0.82 ± 0.02 in filopodia ($n=22$) and 0.74 ± 0.04 in lamellipodia ($n=22$). Surprisingly, colocalization between F-actin and α -actinin was not as strong as expected, with Rr of 0.43 ± 0.03 ($n=22$) in filopodia and 0.29 ± 0.03 in lamellipodia ($n=22$) (Fig. 7c).

We then studied whether the colocalization requires TRPM7 activity. Interestingly, the Rr values of F-actin and α -actinin-1 increased to 0.52 ± 0.03 in filopodia and 0.35 ± 0.03 in lamellipodia in neurons treated with 500 nM waixenicin A for 24 h, and the Rr between TRPM7 and α -actinin decreased to 0.52 ± 0.03 in filopodia and 0.32 ± 0.04 in lamellipodia. Colocalization between TRPM7 and F-actin remained the same as in control neurons (Supplementary Table 1). These findings suggest that TRPM7 is more strongly colocalized with F-actin than with α -actinin in the growth cone. Blocking TRPM7 by waixenicin A reduces TRPM7-to-actinin binding, while enhances (α -actinin)-to-(F-actin) interaction. All of the colocalization data are summarized in Supplementary Table 1.

To determine whether chronic treatment of waixenicin A affects expression levels of the proteins, we measured α -actinin level in the untreated, vehicle-treated, and waixenicin A-treated neurons (24-h treatment) and found no significant differences in protein levels (Fig. 7d). Thus, it is likely that the changes in colocalization between TRPM7 and actinin were due to spatial rearrangement of α -actinin. Taken together, our observations suggest that TRPM7 forms a potential complex with F-actin and α -actinin-1 that could be involved in

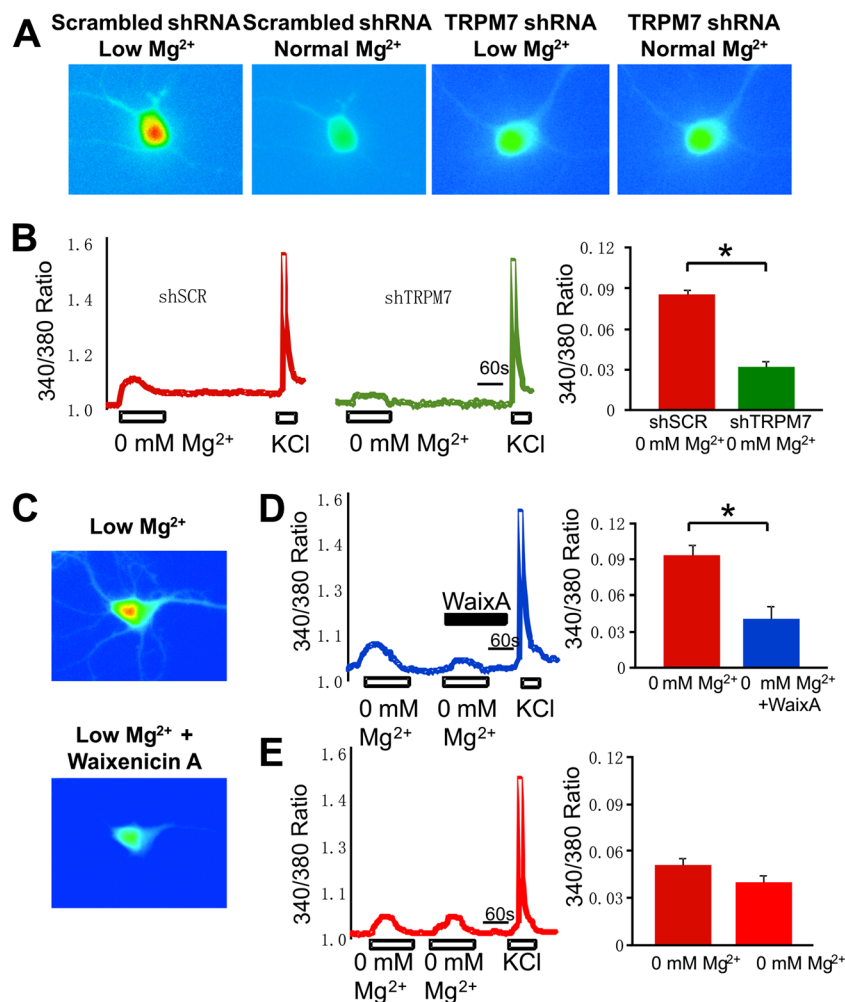


Fig. 6 Calcium influx through TRPM7 is reduced in TRPM7 knockdown and waixenicin A-treated neurons. **a** Representative calcium images show that Mg^{2+} -free and low Ca^{2+} application induce a smaller Ca^{2+} influx in TRPM7 shRNA transduced neurons than in neurons treated with scrambled shRNA. **b** Representative 340/380 ratio traces of neurons transduced with scrambled shRNA (left panel) or TRPM7 shRNA (middle panel); average peak 340/380 ratio values of TRPM7-induced calcium influx (right panel). **c** Representative images of control and waixenicin A-treated neurons. **d** Representative 340/380 ratio trace of neurons perfused with Mg^{2+} -free solution followed by Mg^{2+} -free

solution together with 500 nM waixenicin A (left panel); average peak 340/380 ratio values of TRPM7-induced calcium influx (right panel). **e** Representative 340/380 ratio trace of two consecutive applications of Mg^{2+} -free solution to hippocampal neurons (left panel) and average peak 340/380 ratio values of TRPM7-induced calcium influx (right panel). For scrambled shRNA neurons $n=16$, TRPM7 shRNA neurons $n=16$, untreated neurons $n=10$, waixenicin A-treated neurons $n=10$, control neurons $n=19$. Data are presented as mean \pm SEM. Statistical analysis: one-way ANOVA with Bonferroni post hoc; $*p<0.05$

regulation of neurite growth. Blocking TRPM7 activity brings F-actin and α -actinin-1 into closer proximity, which allows for stronger anchoring of F-actin to the membrane and enhanced neurite outgrowth.

Discussion

In this study, we demonstrate for the first time that calcium-permeable, constitutively active TRPM7 channels participate in regulating neurite outgrowth and maturation, with preferential effect on axonal growth and branching, using genetic

and pharmacological approaches. We confirmed that both knockdown of TRPM7 with shRNA and specific blocking of TRPM7 by waixenicin A promote neurite outgrowth in embryonic hippocampal neuronal culture. We also demonstrate TRPM7 expression pattern in neuronal growth cones and propose a model for TRPM7-mediated axonal outgrowth.

TRPM7 Expression in Hippocampal Neurons Suggests a Developmental Function

Several studies demonstrated TRPM7 expression patterns in different types of mammalian neurons in vitro. In mouse and rat hippocampal neurons, TRPM7 showed a diffused

expression pattern in the cell bodies and processes [4, 25]. In hippocampal neurons, broader TRPM7 expression correlates well with its role in divalent ion homeostasis [25] and cell survival [4]. In this study, we showed that TRPM7 is expressed in the growth cones of mouse hippocampal neurons. Since the growth cone is a key structure responsible for axonal navigation in developing nervous system, TRPM7 expression patterns shown in this study suggests a specific developmental role.

TRPM7 Maintains Proper Axonal Development by Inhibiting Excessive Growth and Premature Axonal Specification

Neuronal differentiation is essential to nervous system development and function. Development of cultured hippocampal neurons has been characterized and separated into several stages, starting from neuronal sprouting followed by axonal specification and elongation [14]. Growth cones, highly dynamic structures at the tips of elongating neurites, act as “vehicles” which move the protruding neurites toward their ultimate targets [31].

Here, we utilized pharmacological and genetic (AAV vector) approaches to study the role of TRPM7 channels in neuronal development. We report that either shRNA knockdown of TRPM7 or TRPM7 conductance blocked by waixenicin A promoted axonal outgrowth and enhanced axonal specification by enhancing neuronal polarization. We also report that blockade of TRPM7 enhances axonal branching, while shRNA knockdown does not have a significant effect on the number of neurites. This difference could be due to the fact that physical presence of TRPM7 is required for the branching process; thus, further studies are required to elucidate the role of TRPM7 in axonal branching. Our data describe that under physiological conditions TRPM7 channel functions as an inhibitor of axonal outgrowth and maturation. As these processes are crucial for proper target finding and formation of functional neuronal networks, they must be tightly regulated to avoid overgrowth and connection with unwanted targets. Indeed, postmortem analysis of brain tissue from individuals with autism showed excessive axonal branching in several prefrontal areas associated with attention, emotions, and social interactions [32]. In fact, the maintenance of axonal morphology is an active process that requires constant suppression of sprouting through limiting actin polymerization along the neurite shaft by calpain proteases [33]. Thus, TRPM7 proteins represent one of the potential mechanisms for regulation of proper axonal outgrowth.

TRPM7 Blockers

While shRNA approach has been successfully utilized in studying TRPM7 channels in neurons [3, 4], the earliest time point at which channel knockdown can be reliably achieved is

DIV4. Thus, it was impossible for us to observe the effects of TRPM7 knockdown on early developmental events, such as sprouting and axonal specification. In addition, this approach affects the amount of protein expressed by the cell, and thus does not allow for testing functional role of the channel as an ion entryway.

The progress of TRPM7 research was impeded by the lack of selective TRPM7 antagonists [34]. Previous studies used non-specific blockers, such as Gd^{3+} [3], 2-aminoethoxydiphenyl borate (2-APB) [35], nordihydroguaiaretic acid (NDGA), AA861, MK886 [36], carvacrol [37], and sphingosine and its synthetic analogue FTY720 [38] to study its physiological and pathophysiological roles. However, these blockers were shown to affect other TRP and calcium-conducting channels [35, 37–40].

Waixenicin A [23] is a diterpene from the Hawaiian soft coral *Sarcothelia edmondsoni* and a highly potent specific blocker of TRPM7. It does not affect other closely related TRPM channels, such as TRPM6, TRPM2, and TRPM4 [23]. In our hands, the IC_{50} value in primary hippocampal neuronal culture was almost 20 times greater than that of recombinant TRPM7 expressed in HEK-293 cells [23]. Endogenous TRPM7 often forms heteromers with TRPM6 [41], which may affect the binding of the blocker to the channel [42].

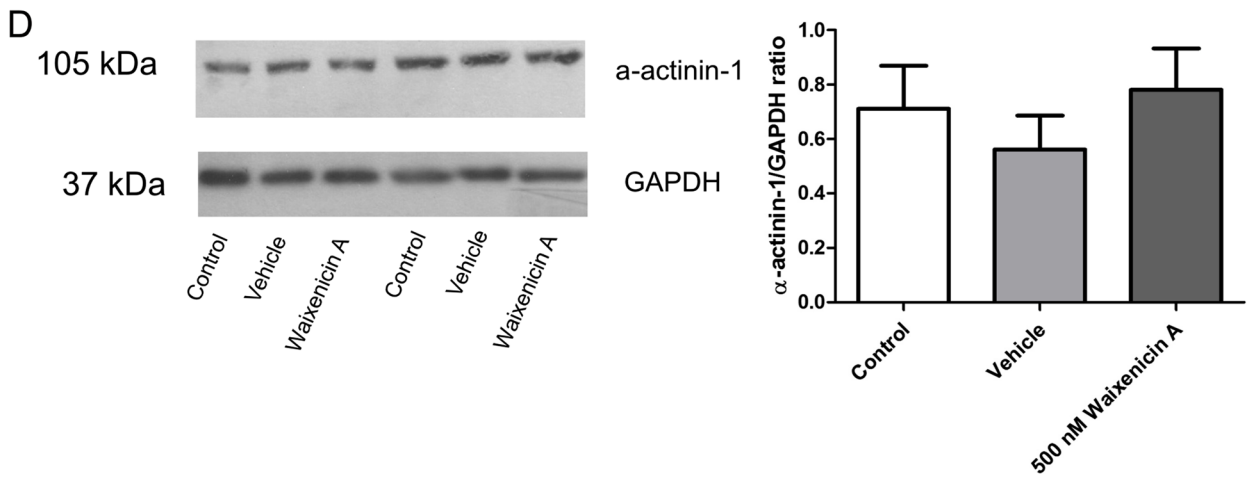
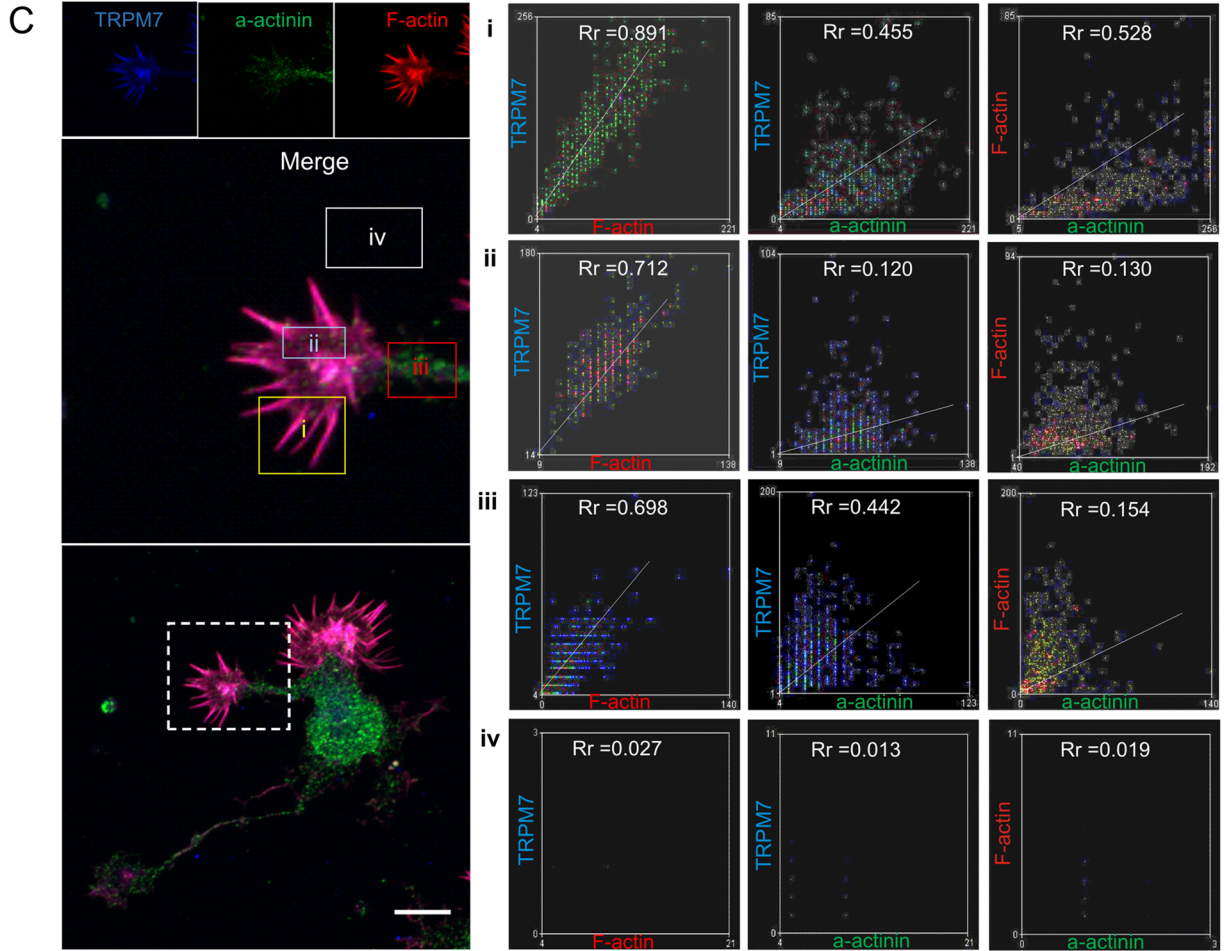
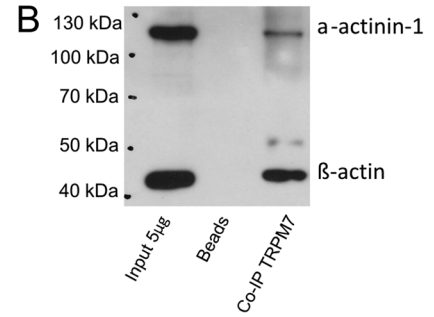
TRPM7 Regulates Axonal Outgrowth Through Calcium Influx

We show that both shRNA knockdown and TRPM7 conductance block led to comparable increases in axonal outgrowth. We also show that TRPM7 block by waixenicin A causes a similar decrease in calcium influx ($58 \pm 8\%$ decrease) as compared to TRPM7 shRNA knockdown ($62 \pm 4\%$ decrease). These results suggest that calcium influx through TRPM7 plays a greater role in neurite outgrowth regulation than physical presence of the protein, as cytoskeletal dynamics at the growth cone are tightly controlled by local intracellular calcium levels [15–17], which in turn regulates neurite elongation and motility [18, 19]. Nevertheless, the role of TRPM7 as a scaffolding protein cannot be ruled out completely.

Moreover, previous study has also shown that magnesium influx through TRPM7 channels can modulate cell proliferation in DT40 B cells [12]. As magnesium is an important regulator of the cytoskeleton [43], it is possible that magnesium influx through TRPM7 contributes to TRPM7-mediated neurite outgrowth. Under low magnesium conditions, TRPM7 via its C-terminal kinase domain [44] enhances phosphorylation of eukaryotic elongation factor 2 kinase (eEF2K) [45]. Phosphorylation of eEF2 inhibits protein synthesis at developing synapse [46]. The increase in axonal outgrowth by TRPM7 inhibition could be through suppression of eEF2K phosphorylation. Our findings support the notion of TRPM7 functions as a negative regulator to mediate optimal axonal

A

Identified Proteins	SCORE (Control)	SCORE (Pull-down)	Confidence Level (Probability)	Functions
Actin, cytoplasmic 1	6	9	>95%	Major cytoskeletal protein.
Alpha-actinin-1	1	4	>95%	F-actin cross-linking protein which is thought to anchor actin to a variety of intracellular structures. EF-hand domain



◀ **Fig. 7** TRPM7 coprecipitates with actin and α -actinin-1. **a** Mass spectroscopy analysis of coimmunoprecipitation with anti-TRPM7 antibody from protein isolated from mouse hippocampal tissue. **b** β -Actin and α -actinin-1 coimmunoprecipitate with TRPM7 in protein isolated from MDA-MB-231 cells. **c** Protein colocalization analysis using fluorescence correlation analysis indicates strong colocalization between TRPM7 and F-actin and moderate colocalization between TRPM7 and α -actinin-1 and between F-actin and α -actinin-1. *Rr* Pearson's correlation coefficient. *Scale bar* is 20 μ m. **d** Western blot analysis indicates that protein levels of α -actinin-1 do not significantly differ between control and waixenicin A-treated groups ($n=4$ for each group, one-way ANOVA followed by Bonferroni post hoc). Data are shown as mean \pm SEM

outgrowth. While a significant cytoskeletal rearrangement at the growth cone or change in expression of cytoskeleton-mediating proteins due to TRPM7 downregulation cannot be ruled out as potential reasons for observed axonal outgrowth, they are beyond the scope of this study.

A Model for TRPM7-Mediated Axonal Outgrowth via Interactions with Actin and Actinin

Actin dynamics at the elongating growth cone are locally and tightly regulated by actin-mediating proteins in response to guidance cues, adhesive/repulsive substrate encounters, and calcium fluxes [47]. This regulation of actin assembly, turnover, and interactions with the membrane and cytoskeleton are critical in generating the traction and pulling force needed to navigate the elongating neurite toward its target [47]. Here, we show that TRPM7 interacts and colocalizes with the cytoskeletal protein actin, and actin-binding protein α -actinin-1. Our data support the notion that TRPM7 mediates axonal outgrowth via actin and α -actinin-1 protein complex, or a TRPM7-mediated protein microdomain in the growth cone. This microdomain regulates actin anchoring by α -actinin-1 and calcium influx through TRPM7. Actin anchoring affects actin polymerization, which is crucial in filopodial protrusion and growth cone motility [20]. Suppressing TRPM7 activity by waixenicin A would allow for greater interaction between F-actin and α -actinin-1, thus enhancing growth cone filopodial protrusion and leading to increased neurite outgrowth, branch formation, and axonal differentiation. On the other hand, potentiation of TRPM7 current would cause dissociation of F-actin from the membrane leading to axonal degeneration and growth cone collapse.

TRPM7 May Serve as Mechanosensor During Neuronal Development

The regulatory role of TRPM7 in neurite elongation can be explained by mechanosensitive nature of the channel [48]. Stretch-activated channels (SACs) were long thought to be candidates for regulating growth cone motility in neurons [49, 50]. It was proposed that SACs regulate neurite outgrowth by mediating local calcium dynamics within specific growth

cone microdomains [50]. These microdomains are functionally linked to specific calcium-sensitive effectors that regulate cytoskeletal rearrangement at the growth cone [50]. Blocking these stretch-activated channels accelerates axonal outgrowth, however, their identity remains unknown [50]. Previous study with migrating embryonic lung fibroblasts has shown that TRPM7 transduces the local mechanical stress into an intracellular calcium signals in the form of calcium flickers at the leading end of migrating cells [48]. Our results further support the hypothesis of TRPM7 channels function as a mechanosensitive regulator of neuronal cytoskeleton. Therefore, it is conceivable that the extent of growth cone protrusion and neurite elongation would depend on a ratio of open to closed TRPM7 channels.

In conclusion, our study opens the field for investigation of potential mechanisms of the TRPM7-mediated regulation of neurite outgrowth and maturation. These mechanisms will lead to potential identification of new therapeutic targets for neurological disorders caused by disrupted axonal growth, branching, or pathfinding, as well as neuronal regeneration after injury.

Acknowledgments This work was supported by the following grants: NIH NIGMS P01 (GM078195) to AF, Natural Sciences and Engineering Research Council of Canada (NSERC) Discovery Grants to ZPF (RGPIN 249962) and to HSS (RGPIN 402733), a Canada Foundation for Innovation (CFI #29066) Leader of Opportunity Fund and Ontario Research Fund (ORF) to HSS, a Canadian Institute of Health Research (CIHR) Frederick Banting and Charles Best Canada Graduate Scholarship to ET, Ontario Graduate Scholarships to CB (OGS-MSc) and to AB (OGS-PhD), and a New Investigator Award from the Heart and Stroke Foundation of Canada (HSFC) to ZPF.

References

1. Clapham DE, Julius D, Montell C, Schultz G (2005) International union of pharmacology. XLIX. Nomenclature and structure-function relationships of transient receptor potential channels. *Pharmacol Rev* 57:427–450
2. Fleig A, Chubakov V (2014) Trpm7. *Handb Exp Pharmacol* 222: 521–546
3. Aarts M, Iihara K, Wei WL, Xiong ZG, Arundine M, Cerwinski W, MacDonald JF, Tymianski M (2003) A key role for TRPM7 channels in anoxic neuronal death. *Cell* 115:863–877
4. Sun HS, Jackson MF, Martin LJ, Jansen K, Teves L, Cui H, Kiyonaka S, Mori Y, Jones M, Forder JP, Golde TE, Orser BA, MacDonald JF, Tymianski M (2009) Suppression of hippocampal TRPM7 protein prevents delayed neuronal death in brain ischemia. *Nat Neurosci* 12: 1300–1307
5. Monteilh-Zoller MK, Hermosura MC, Nadler MJ, Scharenberg AM, Penner R, Fleig A (2003) TRPM7 provides an ion channel mechanism for cellular entry of trace metal ions. *J Gen Physiol* 121:49–60
6. Ryazanova LV, Rondon LJ, Zierler S, Hu Z, Galli J, Yamaguchi TP, Mazur A, Fleig A, Ryazanov AG (2010) TRPM7 is essential for Mg(2+) homeostasis in mammals. *Nat Commun* 1:109
7. Inoue K, Branigan D, Xiong ZG (2010) Zinc-induced neurotoxicity mediated by transient receptor potential melastatin 7 channels. *J Biol Chem* 285:7430–7439

8. Hanano T, Hara Y, Shi J, Morita H, Umebayashi C, Mori E, Sumimoto H, Ito Y, Mori Y, Inoue R (2004) Involvement of TRPM7 in cell growth as a spontaneously activated Ca²⁺ entry pathway in human retinoblastoma cells. *J Pharmacol Sci* 95:403–419
9. Brauchi S, Krapivinsky G, Krapivinsky L, Clapham DE (2008) TRPM7 facilitates cholinergic vesicle fusion with the plasma membrane. *Proc Natl Acad Sci U S A* 105:8304–8308
10. Krapivinsky G, Mochida S, Krapivinsky L, Cibulsky SM, Clapham DE (2006) The TRPM7 ion channel functions in cholinergic synaptic vesicles and affects transmitter release. *Neuron* 52:485–496
11. Clark K, Langeslag M, Van LB, Ran L, Ryazanov AG, Figdor CG, Moolenaar WH, Jalink K, van Leeuwen FN (2006) TRPM7, a novel regulator of actomyosin contractility and cell adhesion. *EMBO J* 25:290–301
12. Nadler MJ, Hermosura MC, Inabe K, Perraud AL, Zhu Q, Stokes AJ, Kurotaki T, Kinet JP, Penner R, Scharenberg AM, Fleig A (2001) LTRPC7 is a Mg²⁺-ATP-regulated divalent cation channel required for cell viability. *Nature* 411:590–595
13. Jin J, Desai BN, Navarro B, Donovan A, Andrews NC, Clapham DE (2008) Deletion of *Trpm7* disrupts embryonic development and thymopoiesis without altering Mg²⁺ homeostasis. *Science* 322:756–760
14. Dotti CG, Sullivan CA, Banker GA (1988) The establishment of polarity by hippocampal neurons in culture. *J Neurosci* 8:1454–1468
15. Gomez TM, Spitzer NC (2000) Regulation of growth cone behavior by calcium: new dynamics to earlier perspectives. *J Neurobiol* 44:174–183
16. Lohmann C, Finski A, Bonhoeffer T (2005) Local calcium transients regulate the spontaneous motility of dendritic filopodia. *Nat Neurosci* 8:305–312
17. Montell C (2005) The latest waves in calcium signaling. *Cell* 122:157–163
18. Mattson MP, Kater SB (1987) Calcium regulation of neurite elongation and growth cone motility. *J Neurosci* 7:4034–4043
19. Henley J, Poo MM (2004) Guiding neuronal growth cones using Ca²⁺ signals. *Trends Cell Biol* 14:320–330
20. Forscher P, Smith SJ (1988) Actions of cytochalasins on the organization of actin filaments and microtubules in a neuronal growth cone. *J Cell Biol* 107:1505–1516
21. BurrIDGE K, Feramisco JR (1981) Non-muscle alpha actinins are calcium-sensitive actin-binding proteins. *Nature* 294:565–567
22. Fu X, Brown KJ, Yap CC, Winckler B, Jaiswal JK, Liu JS (2013) Doublecortin (*Dcx*) family proteins regulate filamentous actin structure in developing neurons. *J Neurosci* 33:709–721
23. Zierler S, Yao G, Zhang Z, Kuo WC, Porzgen P, Penner R, Horgen FD, Fleig A (2011) Waixenicin A inhibits cell proliferation through magnesium-dependent block of transient receptor potential melastatin 7 (TRPM7) channels. *J Biol Chem* 286:39328–39335
24. Gardzinski P, Lee DW, Fei GH, Hui K, Huang GJ, Sun HS, Feng ZP (2007) The role of synaptotagmin I C2A calcium-binding domain in synaptic vesicle clustering during synapse formation. *J Physiol* 581:75–90
25. Wei WL, Sun HS, Olah ME, Sun X, Czerwinska E, Czerwinski W, Mori Y, Orser BA, Xiong ZG, Jackson MF, Tymianski M, MacDonald JF (2007) TRPM7 channels in hippocampal neurons detect levels of extracellular divalent cations. *Proc Natl Acad Sci U S A* 104:16323–16328
26. Nejatbakhsh N, Guo CH, Lu TZ, Pei L, Smit AB, Sun HS, van Kesteren RE, Feng ZP (2011) Caltubin, a novel molluscan tubulin-interacting protein, promotes axonal growth and attenuates axonal degeneration of rodent neurons. *J Neurosci* 31:15231–15244
27. Schmitz SK, Hjorth JJ, Joemai RM, Wijntjes R, Eijgenraam S, De BP, Georgiou C, de Jong AP, Van OA, Verhage M, Cornelisse LN, Toonen RF, Veldkamp WJ (2011) Automated analysis of neuronal morphology, synapse number and synaptic recruitment. *J Neurosci Methods* 195:185–193
28. Silverman-Gavrila LB, Lu TZ, Prashad RC, Nejatbakhsh N, Charlton MP, Feng ZP (2009) Neural phosphoproteomics of a chronic hypoxia model—*Lymnaea stagnalis*. *Neuroscience* 161:621–634
29. Bentley D, Toroian-Raymond A (1986) Disoriented pathfinding by pioneer neurone growth cones deprived of filopodia by cytochalasin treatment. *Nature* 323:712–715
30. Middelbeek J, Kuipers AJ, Henneman L, Visser D, Eidhof I, Van HR, Wieringa B, Canisius SV, Zwart W, Wessels LF, Sweep FC, Bult P, Span PN, van Leeuwen FN, Jalink K (2012) TRPM7 is required for breast tumor cell metastasis. *Cancer Res* 72:4250–4261
31. Lowery LA, Van VD (2009) The trip of the tip: understanding the growth cone machinery. *Nat Rev Mol Cell Biol* 10:332–343
32. Zikopoulos B, Barbas H (2010) Changes in prefrontal axons may disrupt the network in autism. *J Neurosci* 30:14595–14609
33. Mingorance-Le MA, O'Connor TP (2009) Neurite consolidation is an active process requiring constant repression of protrusive activity. *EMBO J* 28:248–260
34. Schmitz C, Perraud AL, Johnson CO, Inabe K, Smith MK, Penner R, Kurotaki T, Fleig A, Scharenberg AM (2003) Regulation of vertebrate cellular Mg²⁺ homeostasis by TRPM7. *Cell* 114:191–200
35. Li M, Jiang J, Yue L (2006) Functional characterization of homo- and heteromeric channel kinases TRPM6 and TRPM7. *J Gen Physiol* 127:525–537
36. Chen HC, Xie J, Zhang Z, Su LT, Yue L, Runnels LW (2010) Blockade of TRPM7 channel activity and cell death by inhibitors of 5-lipoxygenase. *PLoS One* 5:e11161
37. Parnas M, Peters M, Dadon D, Lev S, Vertkin I, Slutsky I, Minke B (2009) Carvacrol is a novel inhibitor of *Drosophila* TRPL and mammalian TRPM7 channels. *Cell Calcium* 45:300–309
38. Qin X, Yue Z, Sun B, Yang W, Xie J, Ni E, Feng Y, Mahmood R, Zhang Y, Yue L (2013) Sphingosine and FTY720 are potent inhibitors of the transient receptor potential melastatin 7 (TRPM7) channels. *Br J Pharmacol* 168:1294–1312
39. Grimm C, Kraft R, Schultz G, Harteneck C (2005) Activation of the melastatin-related cation channel TRPM3 by D-erythro-sphingosine [corrected]. *Mol Pharmacol* 67:798–805
40. Ozaki T, Mohammad S, Morioka E, Takiguchi S, Ikeda M (2013) Infant satiety depends on transient expression of cholecystokinin-1 receptors on ependymal cells lining the third ventricle in mice. *J Physiol* 591:1295–1312
41. Schmitz C, Dorovkov MV, Zhao X, Davenport BJ, Ryazanov AG, Perraud AL (2005) The channel kinases TRPM6 and TRPM7 are functionally nonredundant. *J Biol Chem* 280:37763–37771
42. Zhang Z, Yu H, Huang J, Faouzi M, Schmitz C, Penner R, Fleig A (2014) The TRPM6 kinase domain determines the Mg²⁺-ATP sensitivity of TRPM7/M6 heteromeric ion channels. *J Biol Chem* 289:5217–5227
43. Prescott AR, Comerford JG, Magrath R, Lamb NJ, Warn RM (1988) Effects of elevated intracellular magnesium on cytoskeletal integrity. *J Cell Sci* 89(Pt 3):321–329
44. Krapivinsky G, Krapivinsky L, Manasian Y, Clapham DE (2014) The TRPM7 chanzyme is cleaved to release a chromatin-modifying kinase. *Cell* 157:1061–1072
45. Perraud AL, Zhao X, Ryazanov AG, Schmitz C (2011) The channel-kinase TRPM7 regulates phosphorylation of the translational factor eEF2 via eEF2-k. *Cell Signal* 23:586–593
46. Scheetz AJ, Nairn AC, Constantine-Paton M (2000) NMDA receptor-mediated control of protein synthesis at developing synapses. *Nat Neurosci* 3:211–216
47. Gomez TM, Letourneau PC (2014) Actin dynamics in growth cone motility and navigation. *J Neurochem* 129:221–234
48. Wei C, Wang X, Chen M, Ouyang K, Song LS, Cheng H (2009) Calcium flickers steer cell migration. *Nature* 457:901–905
49. Sigurdson WJ, Morris CE (1989) Stretch-activated ion channels in growth cones of snail neurons. *J Neurosci* 9:2801–2808
50. Jacques-Fricke BT, Seow Y, Gottlieb PA, Sachs F, Gomez TM (2006) Ca²⁺ influx through mechanosensitive channels inhibits neurite outgrowth in opposition to other influx pathways and release from intracellular stores. *J Neurosci* 26:5656–5664